Two-Step Photoalignment with High Resolution for the Alignment of Blue Phase Liquid Crystal

*Sunqian Liu, Inge Nys, Kristiaan Neyts**

ABSTRACT

The self-assembling properties of liquid crystal (LC) are ideal for realizing switchable optical components. The three-dimensional director organization of the LC is strongly determined by the alignment at the substrate interfaces. Photoalignment is a versatile method involving exposure of a photosensitive layer with linearly polarized UV light. Thanks to the rewritability of the photoalignment process, the preferred alignment orientation obtained after a first exposure can be adjusted to obtain more complex patterns. This allows great freedom in the design of alignment patterns for optical devices. In this work, we propose a two-step photoalignment procedure to pattern the alignment at the surface. Illuminations with uniform polarization or with an interference pattern are combined. Stripe patterns and square patterns, with respectively one- and two-dimensional alignment variation, are imposed at the surfaces. We confirm by polarization microscopy that the director of nematic LC can follow the varying azimuthal orientation of a stripe pattern or a square pattern, according to the interference illumination. By increasing the angle between the two interfering beams, photoalignment with high resolution is obtained, compatible with the dimension of the unit cell of blue phase liquid crystals (BPLCs). Stripe patterns with different periodicity and square patterns are investigated. Homogeneous domains of blue phase *II* with (100) or (110) crystal orientation are obtained and their Kossel patterns are recorded. The two-step photoalignment technique allows to create

patterns with high resolution and control the orientation of BPLC, which is promising for a wide range of applications.

KEYWORDS: two-step photoalignment, blue phase liquid crystal, Kossel pattern, high resolution

INTRODUCTION

Liquid crystal (LC) is an organic soft material with orientational order of the long molecular axis, with great potential for tunable optical components. Different LC phases and alignment methods exist to create three-dimensional organizations in a volume.[1-7] There are many ways to align the director, representing the average molecular orientation, at the surfaces of a container holding the LC. Rubbing with a soft cloth rotating on a cylindrical drum over a polyimide layer is a widely used technique to obtain a homogeneous alignment. In addition e-beam or optical lithography,[8, 9] ion-beam etching[10, 11] and photoalignment[12-21] have been reported to realize a spatial variation of alignment.

In photoalignment, a photosensitive alignment chemical is spin-coated on a substrate, followed by exposure to polarized blue or UV light. Recently, different techniques have been reported to obtain complex photopatterning. In the interference illumination method, often two circularly polarized laser beams are used to generate a pattern of linearly polarized light with variable azimuthal orientation, which allows a limited set of patterns.[17, 19] With the scanning beam method, a laser beam with variable linear polarization and variable diameter can scan over the surface of a photosensitive material.[16] A third method is based on the transformation of a phase delay, caused by a pixel of a spatial light modulator (SLM), into an azimuthal angle of linear polarization.[20, 22]

Three- or four-beam interference has been proposed to extend the set of achievable alignment patterns in the interference setup,[1] as well as separate illumination of the top and bottom substrate before cell assembly.[4, 5, 17, 19, 23] In this work we present an alternative interference approach based on two-step photoalignment. This allows to realize a larger set of illumination patterns with variable alignment and high resolution. The effect of multiple exposures, with different linear polarizations, on the resulting photoalignment has been described in the context of direct write illumination.[16] Depending on the polarization and illumination dose in subsequent illumination steps, complete rewriting of the initial alignment pattern can occur, but the resulting pattern can also be due to a combination of both illumination steps. Shteyner et al. demonstrated that a two-step illumination, with interference illumination based on Lloyd's mirror in the second step, allows to obtain alignment patterns with sub-micrometer resolution (105 nm domain size).[21] A similar scheme based on illumination with two Gaussian beams, is used here to obtain one-dimensional alignment patterns with high resolution. In addition two interference steps are used to create two-dimensional patterns.

Alignment patterns with a sub-micrometer period are especially interesting to align LC phases with an inherent period with similar dimensions, such as short pitch chiral LC or blue phase (BP) LC. Photoalignment of short pitch CLC with the help of sub micrometer alignment patterns has attracted a lot of attention in recent years for the creation of flat optical components.[24-28] Recently a tunable polarization volume grating based on BPLC was demonstrated by Cho et al. with the help of a periodically rotating ($\Lambda = 700\,nm$) alignment grating obtained by one step interference illumination.[29] The blue phase (BP) of liquid crystal typically exhibits sub-micrometer periodicity in three dimensions. This structure can be considered as an arrangement of double-twisted LC cylinders in different types of lattices: a simple cubic lattice for $BPII$ and a body-centered cubic lattice for BPI. The double twist cylinders in a lattice of $BPII$ and BPI are accompanied by intersecting and separated

disclinations respectively. Because of the wavelength scale period, BPLC is well-known for its angle-dependent Bragg reflection in certain wavelength ranges, leading to bright saturated colors in reflection.[18] The presence of a 3D photonic bandgap (for UV or visible light) makes BPLC an excellent candidate for a wide range of applications in photonic and display devices.[30-40] Therefore, it is significant to explore how the BP crystal structure and alignment can be accurately controlled. Due to the non-uniformity and the short period, it is a challenge to obtain full control of the BP alignment. Usually BPLC is infiltrated in a cell without alignment layers[30] or it is aligned by using a homogeneously oriented layer at the surface, either by rubbing or photoalignment.[39, 41, 42] In order to obtain larger domains with homogeneous alignment different procedures have been suggested such as thermal cycling,[43] application of an ac voltage,[36, 44] or a gradient-temperature method.[35] Large mono-domains with tailored lattice orientation have also been stabilized by combining weak surface anchoring with appropriate mixture formulations[45] and reconfiguring into stable orthorhombic and tetragonal lattices has been demonstrated with the help of electrical pulses.[41] Also nano-patterned templates, with chemically patterned substrates with homeotropic/planar anchoring, have been tested to control the BP crystal orientation and photoalignment was used to obtained designed patterning of the crystallographic orientation of the BPLC.[46-48]

Recently periodic alignment has been realized by e-beam lithography[47] or by photoalignment through a mask.[49] With these methods alignment of the BPLC can be obtained, but e-beam lithography comes at a high cost per unit area and the mask alignment needs a high resolution photomask.

Here we propose an alternative method to align BPLC in a large monodomain based on a two-step photoalignment method. Similar to what was proposed before with the help of chemically patterned substrates,[47, 49] the aim is to control monodomain BP lattice orientation by patterning the alignment characteristics with sub-micrometer resolution. We implement a two-step

photoalignment method to impose periodic patterns with sub-micrometer period at the confining substrates. Two patterns with planar alignment and variable azimuthal angle are investigated. The first pattern is a one-dimensional stripe pattern with alignment parallel or perpendicular to the stripes. The second is a two-dimensional square pattern, with orthogonally aligned patches. The orientation of nematic LC and BPLC between two substrates with patterned photoalignment is investigated by polarization optical microscopy (POM) and Kossel pattern analysis.

TWO-STEP PHOTOALIGNMENT

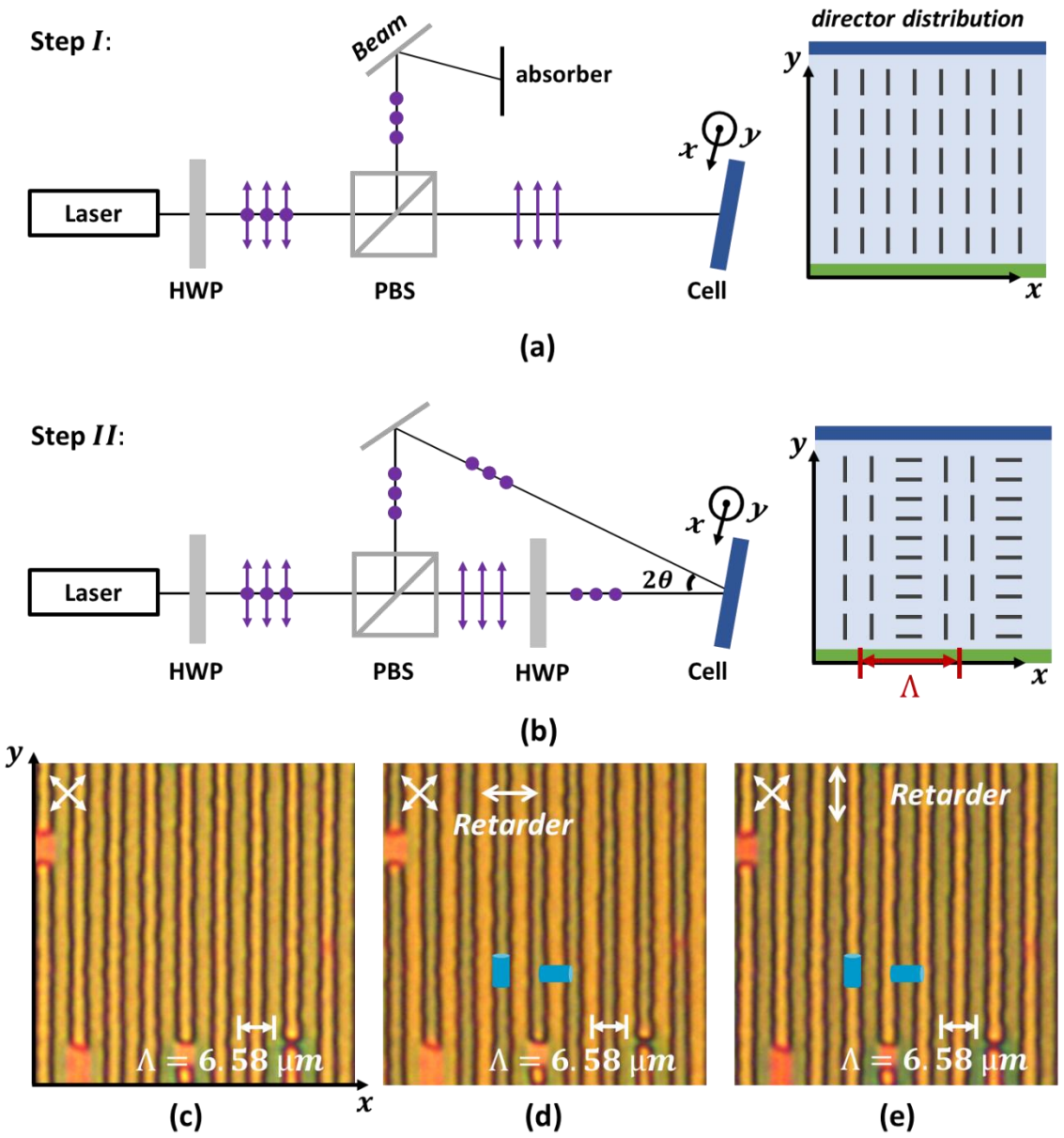

Figure 1. (a)-(b) Set up for two-step photoalignment patterning. Step *I*: homogeneous illumination; Step *II*: interference illumination with two TE beams. **(c)** POM image of the cell after filling with nematic LC. **(d)-(e)** same as in (c) with an added retarder plate with slow axis along *x* or *y*.

We propose a two-step illumination procedure to obtain patterned photoalignment, that enables high resolution. The cell is based on two cleaned glass substrates, which are coated by brilliant

yellow (BY, Sigma Aldrich) and glued together using spherical spacers with diameter of 3 μm according to the Experimental Section. The cell is fixed on a holder for UV exposure. The set-up for illumination consists of a continuous wave UV laser (Coherent, Genesis CX SLM, 100 mW) with wavelength $\lambda = 355\ nm$ and optical components as shown in **Figure 1a-b**. The polarizing beam splitter (PBS) splits the incident beam into two beams with perpendicular polarization, of which the relative intensities are controlled by the half wave plate (HWP) after the laser. In step I (see **Figure 1a**), one beam is blocked by an absorber and the illumination is polarized along the x-axis, leading to a preferred orientation parallel to the y-axis, as BY tends to orient the LC director perpendicularly the polarization of the incident UV light. In step II an additional HWP with fast axis at 45° is added to mirror the polarization of the beam that is used in step I. The two laser beams incident on the cell in step II are polarized along the y-axis (TE polarization) and interfere with each other. By ensuring that the two incident beams have equal power, an interference pattern with maximum modulation is obtained.[21] It means that there are regions parallel to the y-axis with very weak illumination, with spacing $\Lambda = \frac{\lambda}{2 \sin \theta}$ with θ the half angle between the two incident beams. A half angle of 1.54° is used here, corresponding to a period Λ of 6.59 μm. Note that with the method described here it is possible to obtain much shorter periods, because the half angle can easily be increased up to 80° by adding an additional mirror in the setup, as shown in **Figure S1** (Supporting Information). The interference of two TE polarized beams gives rise to pure intensity modulation even for large angles of incidence. In the regions that are not illuminated in step II, we expect the preferred alignment to remain along the y-axis. By choosing an appropriate dose for the interference illumination in the second step, it is possible to obtain regions with approximately equal width having preferred x and y alignment.

After the two-step photoalignment procedure, the nematic LC mixture E7 is injected into the cell above the clearing temperature, and the cell is cooled to room temperature. The transmission is observed by polarized optical microscopy (POM) with crossed polarizers.

When the illumination dose during step II is too low or too high compared to step I, the alignment is more or less homogeneous as shown in **Figure S2** (Supporting Information). When the average dose in step II is about half of that in step I, **Figure 1c-e** shows the periodic pattern observed by POM. The bright regions have the director orientation approximately along the x- or y-axis. In order to distinguish which region has its director along the x-axis, a waveplate with retardation $\Delta n \cdot d = 37\ nm$ is inserted between the crossed polarizers, with slow axis along the x-axis. **Figure 1d** shows that the transmission for the stripes aligned along x shifts to the red, while the color of the other stripe shifts to the green. These shifts are opposite when the slow axis is oriented along y, as shown in **Figure 1e**.The dark stripes between the bright regions indicate that the director becomes parallel to one of the polarizers. When rotating the crossed polarizers, the dark stripes shift, indicating a smooth rotation of the director between x- and y-oriented regions, as illustrated in **Figure S3** (Supporting Information). The period spanning two equivalent bright stripes is $6.58\ \mu m$, in agreement with the value obtained from the illumination setup.

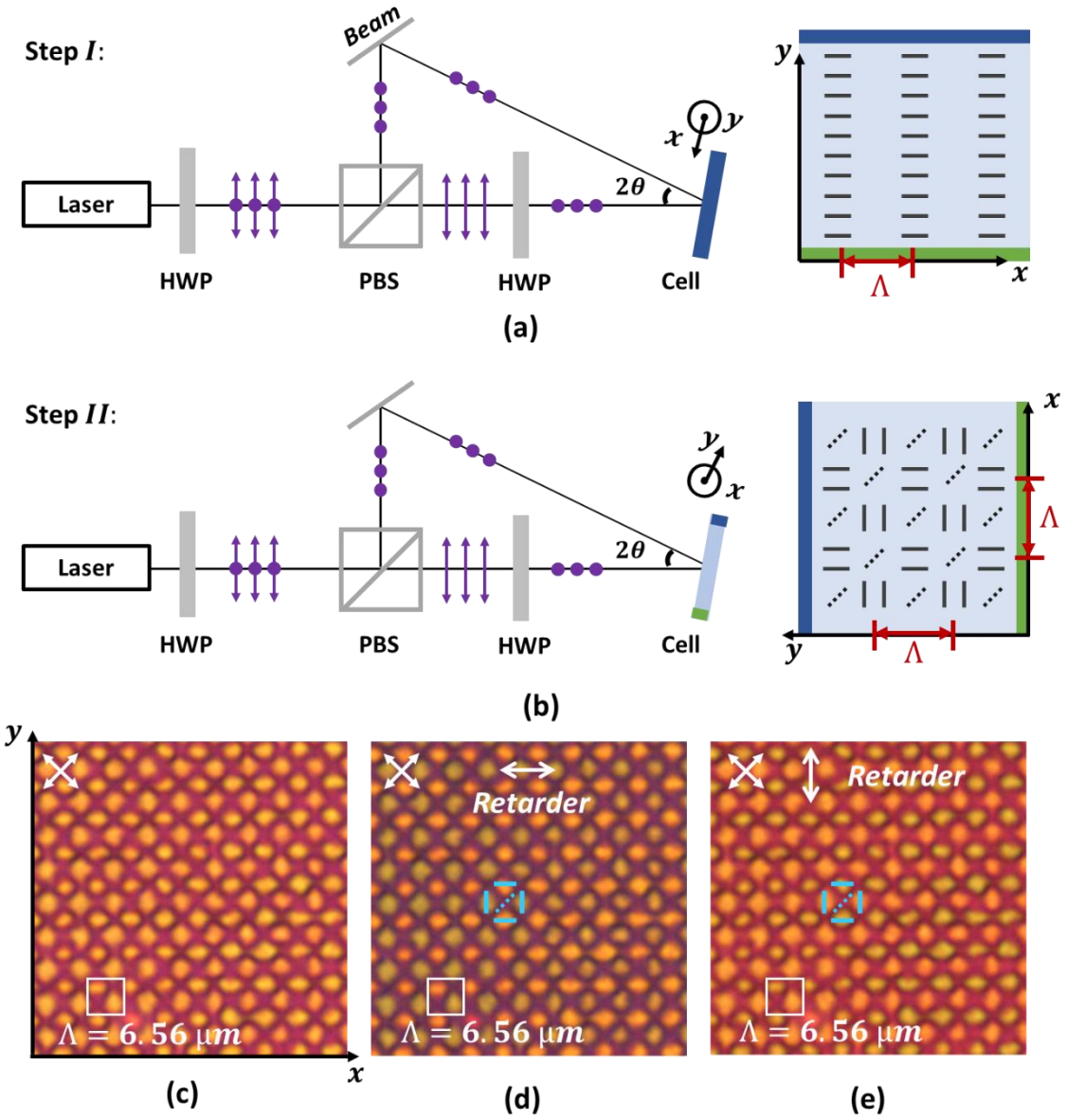

Figure 2. (a)-(b) Set-up for two-step photoalignment with interference in both steps. The cell is rotated over 90 degrees between step *I* and step *II*. **(c)** POM image of a cell after filling with LC. **(d)-(e)** same region as in (c) with a retarder plate with slow axis along *x* or *y* respectively.

The second LC cell is created by using two-step photoalignment with interference illumination in both steps with the same dose (Figure 2), with rotation of the cell over 90° between the two steps. After illumination, the cell is filled with E7 and observed by POM with crossed polarizers.

The POM image in **Figure 2c** shows a matrix of bright orange dots with a dark background. The period in the x- and y-direction, indicated by the white square is 6.56 μm, in agreement with the interference period. In order to identify regions with x- and y-alignment, we add the 37 nm retarder plate with slow axis along the x-axis and obtain **Figure 2d**. Half of the dots undergo a green color shift (reduced retardation, y-alignment), while the others are red-shifted (x-alignment). And the situation is inversed when the retarder is along the y-axis, as shown in **Figure 2e**. Note that it is a challenge to make the two illumination regions match exactly after rotating the cell. As a result the square pattern is only observed in those regions where the ratio of doses is appropriate. Between the patches with x and y orientation, we expect the director to take an orientation along the bisector, as illustrated in **Figure 2d**. The observed POM images are compatible with the schematic pattern in **Figure 2b**, with some patches having alignment along the x-axis (determined by step *I*) and others with alignment along y (determined by step *II*).

PHOTOALIGNMENT OF BPLC

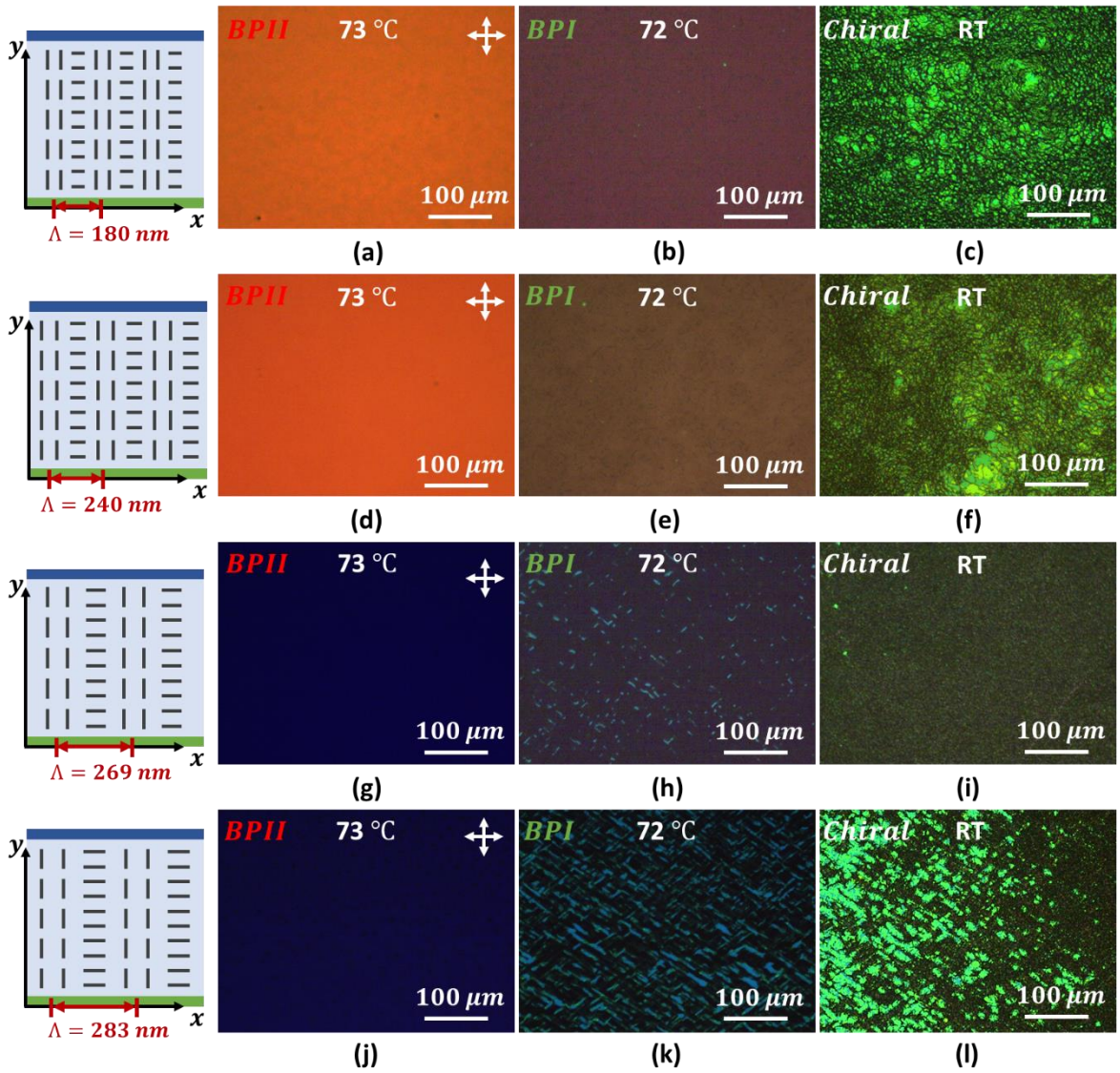

Figure 3. Reflection POM images at different temperatures of BPLC cells with a one-dimensional photoalignment pattern with four different alignment periods Λ. Cooling rate: 0.2 °C/*min*. The period Λ of the photoalignment is 180 *nm* in **(a)-(c)**, 240 *nm* in **(d)-(f)**, 269 *nm* in **(g)-(i)**, and 283 *nm* in **(j)-(l)**.

To align BPLC, photoalignment with a short period and a large angle between the two UV beams is needed, as shown in **Figure S1** (Supporting Information). With the UV laser (wavelength 355 *nm*) the minimal period is 177.5 *nm*, sufficient for most BPLCs. We use the two-step photoalignment approach of **Figure 1** to align a BPLC (label 2044) obtained from

WAT in Warsaw.[44] The angle of incidence is adjusted to obtain the following periods Λ: 180 nm, 240 nm, 269 nm and 283 nm. After the two-step photoalignment procedure of **Figure 1** the cell is filled with BPLC above the clearing temperature and the cell is slowly cooled down (cooling rate: 0.2 ℃/min) in a temperature control stage (STC200, Instec). $BPII$ is obtained around 73 ℃ and BPI is obtained around 72 ℃, while further cooling leads to the cholesteric phase (CLC). **Figure 3** shows reflection POM images of the BPLC between crossed polarizers, for the four devices in the three different phases. For $BPII$, the reflectivity is homogeneous but the color depends on the alignment period: it is orange/red for $\Lambda = 180\ nm$ or $\Lambda = 240\ nm$ and dark blue for the other periods. In BPI, a crosshatched texture can be observed for the patterns with larger period (**Figure 3h, k**).

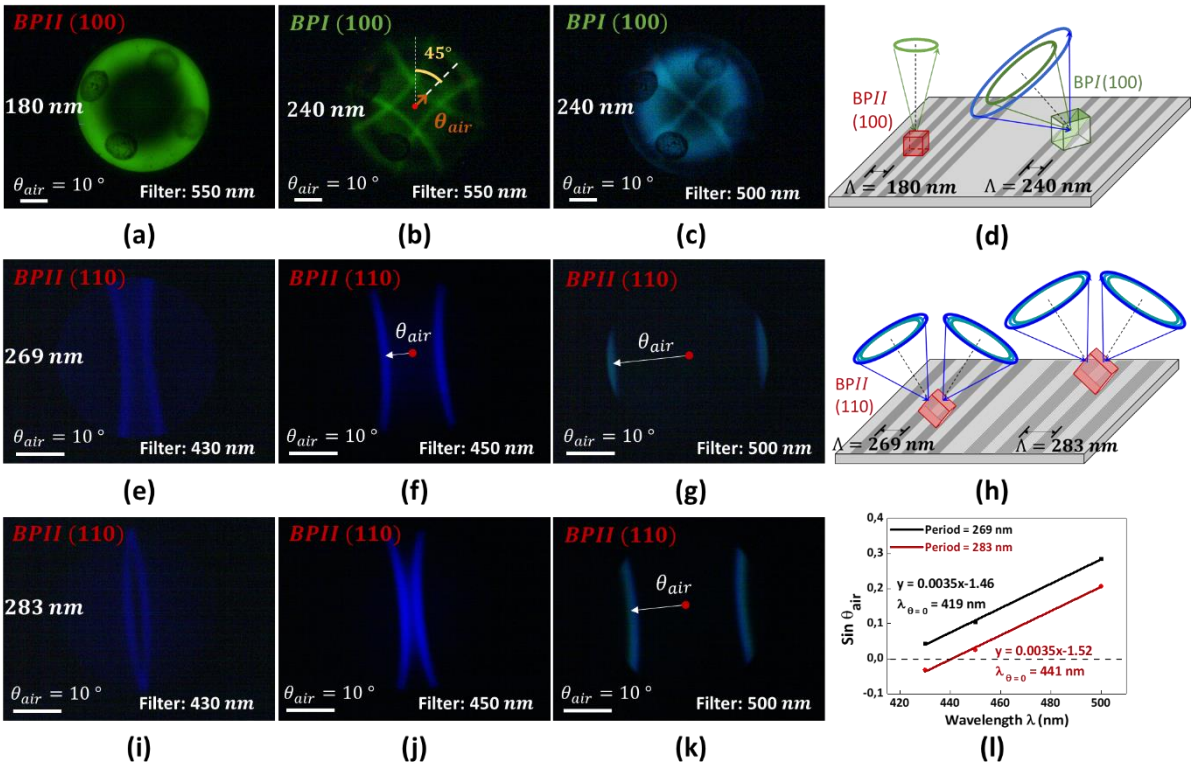

Figure 4. Kossel patterns for BPLC obtained with a Bertrand lens and band pass filter, for $BPII$ (100) with period $\Lambda = 180\ nm$ **(a)**, BPI (100) with $\Lambda = 240\ nm$ **(b)-(c)**, $BPII$ (110) with $\Lambda = 269\ nm$ **(e)-(g)** and $BPII$ (110) with $\Lambda = 283\ nm$ **(i)-(k)**. **(d)-(h)**

Schematic illustration of BPLC cubic unit cell orientation on the patterned alignment layer. **(l)** Relation between the reflection angle θ_{air} and the wavelength for two periods Λ.

The BPLC unit cell orientation is analyzed by measuring the Kossel pattern with reflection microscopy, a Bertrand lens and band-pass filters.[18] The Kossel pattern consists of sections of projected circles, with each circle corresponding to the Bragg reflection from a set of parallel planes (Figure S4, Supporting Information). The scale bar on the Kossel pattern indicates an angle of 10° in air, as explained in **Figure S4** (Supporting Information). Figure 4a shows a ring centered around the origin, indicating reflection on a set of planes parallel with the substrate. The other Kossel images show a set of four equivalent rings (**Figures 4b, c**) or a set of two equivalent rings (**Figure 4e-g** and **i-k**). For each Kossel pattern the shortest distance between the circle and the origin (corresponding to the perpendicular direction) is defined as θ_{air}.

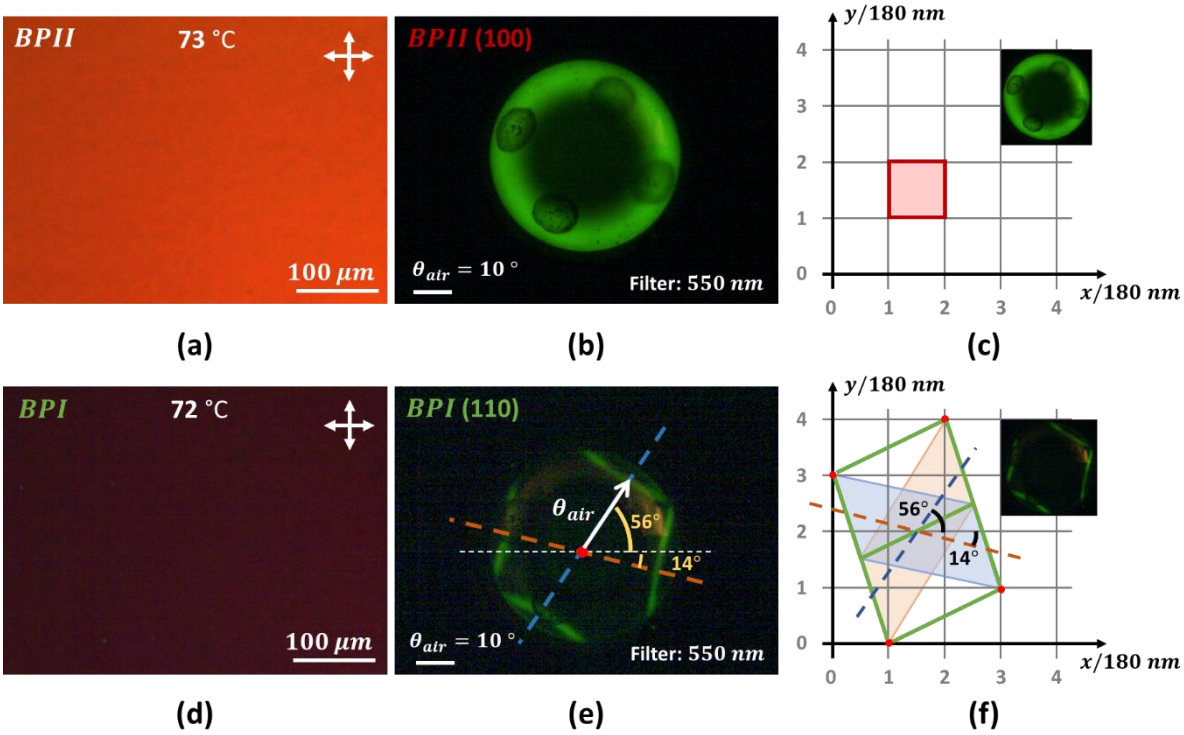

Figure 5. Reflection POM image and corresponding Kossel diagram for BPLC cells obtained

with a square photoalignment grid with period 180 nm, for $BPII$ in **(a)-(b)** and BPI in **(d)-(e)**. **(c)-(f)**: schematic top view of BP unit cell (colored) and photoalignment pattern (black grid).

We now investigate the alignment of BPLC in a cell that has been illuminated by two interference steps. A square photoalignment pattern with period 180 nm is obtained using the illumination as outlined in **Figure 2**. The reflective POM image and corresponding Kossel pattern for $BPII$, obtained around 73 ℃, are shown in **Figures 5a, b**. These results are similar to the results for the linear patterns shown in **Figure 3a** and **4a**. After cooling down to BPI, the reflectivity is lower and the Kossel pattern consists of four circle sections, without four-fold symmetry, as shown in **Figure 5d**, **e**.

DISCUSSION

The period of the one-dimensional interference pattern has an important effect on the BPII alignment, as illustrated in the POM images in **Figure 3a**, **g** and **j** and the Kossel patterns in **Figures 4a**, **e** and **i**. For the period 180 nm the Kossel pattern is a circle with center in the origin, which corresponds to Bragg reflection of planes parallel to the substrate.

The Bragg wavelength λ_B is linked to the Bragg angle θ_B:

$$\lambda_B = 2 \cdot n \cdot d \cdot \cos\theta_B \,. \qquad (1)$$

with n the refractive index of the BPLC ($n \approx 1.55$) and d the distance between the reflection planes. **Figure S4** (Supporting Information) illustrates θ_B and θ_{air} for some reflection planes for $BPII$ and BPI crystals. Assuming a $BPII$ lattice constant a of 180 nm, we find that the Bragg wavelength in the vertical direction $\lambda_B = 2 \cdot n \cdot a = 558\, nm$ corresponds to green reflection. Therefore, the Kossel pattern of **Figure 4a** can be explained by a (100) $BPII$ unit cell orientation as illustrated in **Figure 4d**. When the Bragg reflective planes have a normal that makes an angle θ_N with the substrate normal, then the Bragg reflection circle is not centered around the origin. The minimal angle between the substrate normal and the Bragg reflection

angle in air follows Snell's law. Based on the refractive index n of the BPLC and the inclination angle θ_N of the normal of the reflecting planes, the law of Snell for refraction can be written as:

$$\sin\theta_{air} = n\sin(\theta_N - \theta_B)\,. \qquad (2)$$

For the photoalignment periods 269 nm and 283 nm, the Kossel pattern of $BPII$ shows two circles (**Figure 4e**, **i**). In the literature such patterns are ascribed to a unit cell with (110) orientation[45] due to light reflection from planes that make an angle θ_N of 45 degrees with the substrate, as illustrated in **Figure 4h**. From the wavelength dependency of $\sin\theta_{air}$ in **Figure 4l**, we can find the wavelengths where θ_{air} becomes zero by linear interpolation: 419 nm and 441 nm for the samples with period 269 nm and 283 nm respectively. According to Eq. (2), the Bragg angle θ_B should be 45° for this wavelength, leading to a layer spacing $d = \frac{\lambda_B}{\sqrt{2}\cdot n}$ of 191 nm and 201 nm respectively (Eq. (1)). Note that for the (110) orientation, the period in the substrate plane is $\sqrt{2}\cdot d$, which corresponds to 270 nm and 285 nm respectively, in good agreement with the preset period Λ of the photoalignment patterns. It can be concluded that the linear photoalignment patterns with period 269 nm and 283 nm are not only able to align $BPII$ but also to adjust the lattice constant of the BP.

It is well known that aligning BPI is more challenging, because the crystal has to be formed from $BPII$ during cooling or from the cholesteric phase during heating.[49] In many cases the BPI Kossel diagrams do not provide well-defined lines, indicating that the domains of BPI are small. The clear Kossel patterns in **Figure 4b** and **c** for the photoalignment period $\Lambda = 240\ nm$ indicate that a well-defined BPI phase is created. The four-fold symmetry indicates four sets of planes that yield Bragg reflections. Let us assume that the reflections arise from the four diagonal planes of the cubic cell with inclination angle $\theta_N = 45°$, as illustrated in **Figure 4d**. For the wavelength filter of 500 nm the angle θ_{air} is approximately zero and according to Eq. (2) we have $\theta_B = 45°$. From Eq. (1) we can estimate the distance between the planes $d = \frac{\lambda_B}{\sqrt{2}\cdot n}$

as 228 nm, which corresponds well with the period that we used for the photoalignment. For the lattice constant a of BPI, we find $a = \sqrt{2}d = 323\ nm$, which agrees well with spectra results we reported before.[44] Note that the orientation of the Kossel pattern corresponds to the azimuthal orientation of the cubic cell, with the vertical faces of the cube making an angle of 45 degrees with the stripes of the alignment pattern.

Finally, we discuss the crystal formation of BP on the two-dimensional grid created by two interference illumination steps with period 180 nm. For $BPII$ a domain with (100) orientation is observed. In BPI a particular domain can be created if the lattice points adjust to the period of the square photoalignment grid. **Figure 5f** illustrates how the (110) unit cell of BPI can be slightly deformed to latch the lattice points onto the grid. After the deformation, the unit cell becomes monoclinic (the projection on the xy plane is a parallelogram) and in **Figure 5f** two lattice planes (blue and orange) that can lead to Bragg reflections are indicated. We determine the azimuthal angle of the normal of these planes (dashed blue and orange line) as +56° and -14° with respect to the x-axis. These angles correspond well to the azimuthal angles of the point in the Kossel circle closest to the origin, as can be seen from **Figure 5e**. The distance between the (1,0) and (3,1) grid points is $\sqrt{5} \cdot \Lambda$ or 402 nm (see **Figure 5f**), which is larger than the value estimated from **Figure 4b** (323 nm). This demonstrates that the BPI unit cell that forms on the square photoalignment pattern is stretched and has lost its cubic symmetry.

CONCLUSION

In conclusion, we have demonstrated a two-step method photoalignment method to obtain patterned alignment and monodomain BPLC with preferred lattice orientation. The principle is first demonstrated by writing 1D and 2D photoalignment patterns with low resolution (period 6.5 μm) on photoalignment layers in an empty cell. After filling the cell with nematic LC, we indeed observe corresponding 1D and 2D patterns. By increasing the angle of incidence for the two UV laser beams, 1D and 2D alignment nanopatterns are realized with periods ranging from

180 nm to 283 nm. By injecting BPLC into the cells with nanopatterned photoalignment and slowly cooling down, homogenous BPLC domains are obtained. The BPLC unit cell orientation has been analyzed by polarization microscopy and Kossel pattern measurements. We found that both the orientation and the size of the BPLC unit cell can be modified, in order to obtain large monodomains in which the unit cell matches the periodicity of the photoalignment pattern. It is clear that two-step photoalignment offers great potential to control the alignment and orientation of BPLC in a cheap and versatile way, even for large area devices. This approach to obtain large monodomains may find applications in various electro-optical components or in displays.

METHODS

LC cell preparation. LC cell was based on two glass substrates. The glass substrates were cleaned by ultrasonication for 30 min first in acetone and then in deionized water, followed by drying with nitrogen flow. The cleaned substrates were then subjected to a UV ozone treatment for 15 min. Photoalignment chemical (Brilliant Yellow, Sigma Aldrich) was dissolved in Dimethylformamide (DMF) with a ratio of 0.5 wt%. This solution was spin-coated onto the glass substrates at a speed of 3000 rpm for 30 s, followed by baking at 90 ℃ for 5 min to make the solvent evaporate. Two pretreated substrates were glued together along the edges with a glue (NOA68) that contains spherical spacers with diameter 3 μm.

Photo-patterning. The pretreated cell were irradiated with polarized UV light. The scheme of the set-up is shown in **Figure 1a-b**. A continuous wave UV laser emitting at λ = 355 nm (Coherent, Genesis CX SLM, 100 mW) was used. The laser beam passed through the beam expander and was split by the polarizing beam splitter (PBS). To achieve an alignment layer with high resolution patterns, two-beam interference photopatterning has been reported before.[21] The periodicity depends on the angle between the interfering beams which is governed

by the interference formula $\Lambda = \frac{\lambda}{2\sin\theta}$, with θ the half opening angle between the two interfering beams. Thus, the theoretical limit for the minimum period is $\frac{\lambda}{2} = 177.5\ nm$. A half-wave plate (HWP) is inserted before the PBS with the fast axis at 45°, so that the two beams have equal power.

After photo-patterning, LC monomers were injected into the cell above the isotropic temperature, followed by cooling to room temperature. The alignment of the LC was characterized with the help of a polarizing optical microscope (Nikon Eclipse LV100POL) under crossed polarizers. During POM measurements and Kossel pattern characterization, the temperature of the cell was controlled with the help of a heating stage (STC200, Instec).

Kossel Pattern Characterization. Kossel patterns were observed using a Nikon Eclipse Ci POL polarized microscope (conoscopic image) in reflection, in combination with a Bertrand lens. The illumination system consisted of a halogen lamp and a band-pass interference filter. Four different filters centered around $\lambda_0 = 430\ nm$, $450\ nm$, $500\ nm$ and $550\ nm$ were used to observe the Kossel pattern. For $BPII_{(110)}$, optical Kossel patterns were obtained at the back focal plane of a 20X objective lens (Nikon LWD 20X NA0.40). For $BPII_{(100)}$, $BPI_{(100)}$ and $BPI_{(110)}$, Kossel patterns were obtained using a 100X objective lens (Nikon LWD 100X NA0.90).

Calibration of Kossel patterns. The image of a beam with known angle of incidence was captured by POM in the presence of the Bertrand lens. The position of the beam in the image isused to find the scale in radians per pixel.

ASSOCIATED CONTENT

Supporting Information

The supporting Information is available free of charge.

Additional figures of set up for two-step photoalignment patterning with an added mirror, polarizing optical microscopy images of nematic LC cell fabricated by two-step photoalignment with different illumination conditions, transmission POM for a nematic LC cell for different orientations of the crossed polarizers, schematic illustration of Bragg reflection on particular surfaces in four BPLC unit cells with for different orientations (PDF).

AUTHOR INFORMATION

Corresponding Author

Kristiaan Neyts - Liquid Crystals and Photonics Group, Department of Electronics and Information Systems, Ghent University, Technologiepark-Zwijnaarde 126, Ghent 9052, Belgium; Email: Kristiaan.Neyts@Ugent.be;

Authors

Sunqian Liu - Liquid Crystals and Photonics Group, Department of Electronics and Information Systems, Ghent University, Technologiepark-Zwijnaarde 126, Ghent 9052, Belgium;

Inge Nys - Liquid Crystals and Photonics Group, Department of Electronics and Information Systems, Ghent University, Technologiepark-Zwijnaarde 126, Ghent 9052, Belgium.

Author Contributions

The manuscript was written through contributions of all authors. All authors have given approval to the final version of the manuscript.

Funding Sources

This work was funded by the FWO project (NO. 1S88220N).

Notes

The authors declare no competing financial interest.

ACKNOWLEDGEMENTS

REFERENCES

1. Kawai, K.; Sakamoto, M.; Noda, K.; Sasaki, T.; Kawatsuki, N.; Ono, H. Tunable Dichroic Polarization Beam Splitter Created by One-Step Holographic Photoalignment Using Four-Beam Polarization Interferometry. *J. Appl. Phys.* **2017,** *121*, 013102.

2. Kawai, K.; Sakamoto, M.; Noda, K.; Sasaki, T.; Kawatsuki, N.; Ono, H. Three-Dimensionally Modulated Anisotropic Structure for Diffractive Optical Elements Created by One-Step Three-Beam Polarization Holographic Photoalignment. *J. Appl. Phys.* **2016,** *119*, 123102.

3. Kowalski, B. A.; Guin, T. C.; Auguste, A. D.; Godman, N. P.; White, T. J. Pixelated Polymers: Directed Self Assembly of Liquid Crystalline Polymer Networks. *ACS Macro Lett.* **2017,** *6*, 436-441.

4. Nys, I.; Nersesyan, V.; Beeckman, J.; Neyts, K. Complex Liquid Crystal Superstructures Induced by Periodic Photo-Alignment at Top and Bottom Substrates. *Soft Matter* **2018,** *14*, 6892-6902.

5. Nys, I. Patterned Surface Alignment to Create Complex Three-Dimensional Nematic and Chiral Nematic Liquid Crystal Structures. *Liq. Cryst. Today* **2021,** *29*, 65-83.

6. He, Z.; Tan, G.; Chanda, D.; Wu, S.-T. Novel Liquid Crystal Photonic Devices Enabled by Two-Photon Polymerization [Invited]. *Opt. Express* **2019,** *27*, 11472-11491.

7. Tartan, C. C.; O'Neill, J. J. S.; Salter, P. S.; Aplinc, J.; Booth, M. J.; Ravnik, M.; Morris, S. M.; Elston, S. J. Read on Demand Images in Laser-Written Polymerizable Liquid Crystal Devices. *Adv. Optical Mater.* **2018,** *6*, 1800515.

8. Nys, I.; Beeckman, J.; Neyts, K. Surface-Mediated Alignment of Long Pitch Chiral Nematic Liquid Crystal Structures. *Adv. Optical Mater.* **2018,** *6*, 1800070.

9. Takahashi, H.; Sakamoto, T.; Okada, H. Liquid Crystal Device with 50nm Nanogroove Structure Fabricated by Nanoimprint Lithography. *J. Appl. Phys.* **2010,** *108*, 113529.

10. Palto, S. P.; Geivandov, A. R.; Kasyanova, I. V.; Artemov, V. V.; Gorkunov, M. V. Micro- and Nanostructures for the Spatially Periodic Orientation of Liquid Crystals Obtained by Focused Ion Beam Milling. *JETP Lett.* **2017,** *105*, 174-178.

11. Kasyanova, I. V.; Geivandov, A. R.; Artemov, V. V.; Gorkunov, M. V.; Palto, S. P. Nematic Liquid Crystal Alignment on Subwavelength Metal Gratings. *Beilstein J. Nanotechnol* **2018,** *9*, 42-47.

12. Yaroshchuk, O.; Reznikov, Y. Photoalignment of Liquid Crystals: Basics and Current Trends. *J. Mater. Chem.* **2012,** *22*, 286-300.

13. Chigrinov, V. G. Photoaligning and Photopatterning — a New Challenge in Liquid Crystal Photonics. *Crystals* **2013,** *3*, 149-162.

14. Nys, I.; Chen, K.; Beeckman, J.; Neyts, K. Periodic Planar-Homeotropic Anchoring Realized by Photoalignment for Stabilization of Chiral Superstructures. *Adv. Optical Mater.* **2018,** *6*, 1701163.

15. Guo, Y.; Jiang, M.; Peng, C.; Sun, K.; Yaroshchuk, O.; Lavrentovich, O.; Wei, Q.-H. High-Resolution and High-Throughput Plasmonic Photopatterning of Complex Molecular Orientations in Liquid Crystals. *Adv. Mater.* **2016,** *28*, 2353-2358.

16. Miskiewicz, M. N.; Escuti, M. J. Direct-Writing of Complex Liquid Crystal Patterns. *Opt. Express* **2014,** *22*, 12691-12706.

17. Crawford, G. P.; Eakin, J. N.; Radcliffe, M. D.; Callan-Jones, A.; Pelcovits, R. A. Liquid-Crystal Diffraction Gratings Using Polarization Holography Alignment Techniques. *J. Appl. Phys.* **2005,** *98*, 123102.

18. Bohley, C.; Scharf, T. Matrix Optics Approach for Liquid Crystalline Blue Phases. *Optics and Lasers in Engineering* **2005,** *43*, 329-339.

19. Provenzano, C.; Pagliusi, P.; Cipparrone, G. Electrically Tunable Two-Dimensional Liquid Crystals Gratings Induced by Polarization Holography. *Opt. Express* **2007,** *15*, 5872-5878.

20. Sio, L. D.; Roberts, D. E.; Liao, Z.; Nersisyan, S.; Uskova, O.; Wickboldt, L.; Tabiryan, N.; Steeves, D. M.; Kimball, B. R. Digital Polarization Holography Advancing Geometrical Phase Optics. *Opt. Express* **2016,** *24*, 18297-18306.

21. Shteyner, E. A.; Srivastava, A. K.; Chigrinov, V. G.; Kwok, H.-S.; Afanasyev, A. D. Submicron-Scale Liquid Crystal Photo-Alignment. *Soft Matter* **2013,** *9*, 5160-5165.

22. Berteloot, B.; Nys, I.; Poy, G.; Beeckman, J.; Neyts, K. Ring-Shaped Liquid Crystal Structures through Patterned Planar Photo-Alignment. *Soft Matter* **2020,** *16*, 4999-5008.

23. Nys, I.; Berteloot, B.; Poy, G. Surface Stabilized Topological Solitons in Nematic Liquid Crystals. *Crystals* **2020,** *10*, 840.

24. Kobashi, J.; Yoshida, H.; Ozaki, M. Planar Optics with Patterned Chiral Liquid Crystals. *Nat. Photonics* **2016,** *10*, 389-392.

25. Yin, K.; Zhan, T.; Xiong, J.; He, Z.; Wu, S.-T. Polarization Volume Gratings for near-Eye Displays and Novel Photonic Devices. *Crystals* **2020,** *10*, 561.

26. Chen, P.; Wei, B.-Y.; Hu, W.; Lu, Y.-Q. Liquid-Crystal-Mediated Geometric Phase: From Transmissive to Broadband Reflective Planar Optics. *Adv. Mater.* **2020,** *32*, 1903665.

27. Lee, Y.-H.; Yin, K.; Wu, S.-T. Reflective Polarization Volume Gratings for High Efficiency Waveguide-Coupling Augmented Reality Displays. *Opt. Express* **2017,** *25*, 27008-27014.

28. Nys, I.; Stebryte, M.; Ussembayev, Y. Y.; Beeckman, J.; Neyts, K. Tilted Chiral Liquid Crystal Gratings for Efficient Large-Angle Diffraction. *Adv. Optical Mater.* **2019,** *7*, 1901364.

29. Cho, S.; Yoshida, H.; Ozaki, M. Tunable Polarization Volume Gratings Based on Blue Phase Liquid Crystals. *Opt. Express* **2022,** *30*, 1607-1614.

30. Yokoyama, S.; Mashiko, S.; Kikuchi, H.; Uchida, K.; Nagamura, T. Laser Emission from a Polymer-Stabilized Liquid-Crystalline Blue Phase. *Adv. Mater.* **2006,** *18*, 48-51.

31. Yang, J.; Liu, J.; Guan, B.; He, W.; Yang, Z.; Wang, J.; Ikeda, T.; Jiang, L. Fabrication and Photonic Applications of Large-Domain Blue Phase Films. *J. Mater. Chem. C* **2019,** *7*, 9460-9466.

32. Kim, K.; Hur, S.-T.; Kim, S.; Jo, S.-Y.; Lee, B. R.; Song, M. H.; Choi, S.-W. A Well-Aligned Simple Cubic Blue Phase for a Liquid Crystal Laser. *J. Mater. Chem. C* **2015,** *3*, 5383-5388.

33. Liu, J.; Chen, Y.; Jin, F.; Wang, J.; Ikeda, T.; Jiang, L. Single-, Dual-, Triple, and Quadruple-Wavelength Surface-Emitting Lasing in Blue-Phase Liquid Crystal. *Adv. Mater.* **2022,** *34*, 2108330.

34. Wahle, M.; Brassat, K.; Ebel, J.; Burger, J.; Lindner, J. K. N.; Kitzerow, H.-S. Two-Dimensional Switchable Blue Phase Gratings Manufactured by Nanosphere Lithography. *Opt. Express* **2017,** *25*, 22608-22619.

35. Chen, C.-W.; Hou, C.-T.; Li, C.-C.; Jau, H.-C.; Wang, C.-T.; Hong, C.-L.; Guo, D.-Y.; Wang, C.-Y.; Chiang, S.-P.; Bunning, T. J.; Khoo, I.-C.; Lin, T.-H. Large Three-Dimensional Photonic Crystals Based on Monocrystalline Liquid Crystal Blue Phases. *Nat. Commun.* **2017,** *8*, 727.

36. Chen, Y.; Wu, S.-T. Electric Field-Induced Monodomain Blue Phase Liquid Crystals. *Appl. Phys. Lett.* **2013,** *102*, 171110.

37. Yang, Y.; Zhang, X.; Chen, Y.; Yang, X.; Ma, J.; Wang, J.; Wang, L.; Feng, W. Bioinspired Color-Changing Photonic Polymer Coatings Based on Three-Dimensional Blue Phase Liquid Crystal Networks. *ACS Appl. Mater. Interfaces* **2021,** *13*, 41102-41111.

38. Wang, M.; Zou, C.; Sun, J.; Zhang, L.; Wang, L.; Xiao, J.; Li, F.; Song, P.; Yang, H. Asymmetric Tunable Photonic Bandgaps in Self-Organized 3d Nanostructure of Polymer-Stabilized Blue Phase I Modulated by Voltage Polarity. *Adv. Funct. Mater.* **2017,** *27*, 1702261.
39. Oton, E.; Netter, E.; Nakano, T.; D.-Katayama, Y.; Inoue, F. Monodomain Blue Phase Liquid Crystal Layers for Phase Modulation. *Sci. Rep.* **2017,** *7*, 44575.
40. Jau, H.-C.; Lin, Y.-T.; Li, C.-C.; Chen, C.-W.; Lin, T.-H. Optically Rewritable Dynamic Phase Grating Based on Blue-Phase-Templated Azobenzene Liquid Crystal. *Opt. Express* **2019,** *27*, 10580-10585.
41. Guo, D.-Y.; Chen, C.-W.; Li, C.-C.; Jau, H.-C.; Lin, K.-H.; Feng, T.-M.; Wang, C.-T.; Bunning, T. J.; Khoo, I. C.; Lin, T.-H. Reconfiguration of Three-Dimensional Liquid-Crystalline Photonic Crystals by Electrostriction. *Nat. Mater.* **2020,** *19*, 94-101.
42. Takahashi, M.; Ohkawa, T.; Yoshida, H.; Fukuda, J.-i.; Kikuchi, H.; Ozaki, M. Orientation of Liquid Crystalline Blue Phases on Unidirectionally Orienting Surfaces. *J. Phys. D: Appl. Phys.* **2018,** *51*, 104003.
43. Chen, H.-S.; Lin, Y.-H.; Wu, C.-H.; Chen, M.; Hsu, H.-K. Hysteresis-Free Polymer-Stabilized Blue Phase Liquid Crystals Using Thermal Recycles. *Opt. Mater. Express* **2012,** *2*, 1149-1155.
44. Claus, H.; Willekens, O.; Chojnowska, O.; Dąbrowski, R.; Beeckman, J.; Neyts, K. Inducing Monodomain Blue Phase Liquid Crystals by Long-Lasting Voltage Application During Temperature Variation. *Liq. Cryst.* **2016,** *43*, 688-693.
45. Otón, E.; Yoshida, H.; Morawiak, P.; Strzeżysz, O.; Kula, P.; ozaki, M.; piecek, W. Orientation Control of Ideal Blue Phase Photonic Crystals. *Sci. Rep.* **2020,** *10*, 10148.
46. Martı´nez-Gonza´lez, J. A.; Li, X.; Sadati, M.; Zhou, Y.; Zhang, R.; Nealey, P. F.; Pablo, J. J. d. Directed Self-Assembly of Liquid Crystalline Blue-Phases into Ideal Single-Crystals. *Nat. Commun.* **2017,** *8*, 15854.
47. Li, X.; Martínez-González, J. A.; Park, K.; Yu, C.; Zhou, Y.; Pablo, J. J. d.; Nealey, P. F. Perfection in Nucleation and Growth of Blue-Phase Single Crystals: Small Free-Energy Required to Self-Assemble at Specific Lattice Orientation. *ACS Appl. Mater. Interfaces* **2019,** *11*, 9487-9495.
48. Zheng, Z.-G.; Yuan, C.-L.; Hu, W.; Bisoyi, H. K.; Tang, M.-J.; Liu, Z.; Sun, P.-Z.; Yang, W.-Q.; Wang, X.-Q.; Shen, D.; Li, Y.; Ye, F.; Lu, Y.-Q.; Li, G.; Li, Q. Light-Patterned Crystallographic Direction of a Self-Organized 3d Soft Photonic Crystal. *Adv. Mater.* **2017,** *29*, 1703165.

49. Cho, S.; Takahashi, M.; Fukuda, J.-i.; Yoshida, H.; Ozaki, M. Directed Self-Assembly of Soft 3d Photonic Crystals for Holograms with Omnidirectional Circular-Polarization Selectivity. *Commun. Mater.* **2021,** *2*, 1-9.